Thermoporometry and Proton NMR Measurement on Cement Paste Equilibrated at Different Relative Humidities

Kurumisawa, Kiyofumi; Jensen, Ole Mejlhede

Published in:
Journal of Advanced Concrete Technology

Link to article, DOI:
10.3151/jact.18.456

Publication date:
2020

Document Version
Publisher's PDF, also known as Version of record

Scientific paper

Thermoporometry and Proton NMR Measurement on Cement Paste Equilibrated at Different Relative Humidities

Kiyofumi Kurumisawa[1*] and Ole Mejlhede Jensen[2]

Received 15 June 2020, accepted 29 July 2020 doi:10.3151/jact.18.456

Abstract

In this study, thermoporometry by differential scanning calorimetry and proton NMR measurements of hardened cement paste equilibrated under different humidity conditions were carried out, and the results of both measurements were compared. The results reveal that thermoporometry by low temperature DSC measurement cannot detect the water present in samples equilibrated at low relative humidity. On the other hand, it is possible to detect a signal at low relative humidity by proton NMR measurement. It is clarified that water strongly bound to the surface, which cannot be detected by low temperature DSC, exists at a relative humidity of 33% or less. If it is relevant to detect tightly held water, such as water present in the fine gel pores, it is recommended to apply proton NMR measurements. This paper is an extended English version of the authors' previous work [Kurumisawa, K. and Jensen, O. M., (2020). "Measurement of cement paste at different humidities by thermoporometry and proton NMR." *Proceedings of the Japan Concrete Institute*, 42, 347-352. (in Japanese)].

1. Introduction

In order to improve the durability of concrete structures, it is important to minimize cracking. Since cracks are often caused by drying shrinkage, it is necessary to reduce the amount of shrinkage, and academic societies have thoroughly enforced specifications for this, for example, the Architectural Institute of Japan's specification JASS 5 for reinforced concrete work (AIJ 2018), for example. It is recommended that the drying shrinkage of concrete is less than 800×10^{-6}. To mitigate drying shrinkage and crack formation a deeper understanding of water binding in concrete is needed. In recent years, the development of a method for measuring the state of water in hardened cement-based materials by proton NMR measurement has advanced. By this technique, the specimen can be measured non-destructively, and the state of moisture in concrete can be accessed (Muller *et al.* 2013a, 2013b, 2015; Maruyama *et al.* 2019; Kose *et al.* 2013). Likewise, a technique based on low temperature differential scanning calorimetry (LT-DSC) has also been used to measure the state of water in pores. This so-called thermoporometric method was introduced by Kuhn *et al.* (1955), and further developed by Brun *et al.* (1977). This method has been applied to the behavior of water in porous materials (Brun *et al.* 1977; Ishikiriyama *et al.* 1995; Landry 2005), and applied to hardened cement paste. The method is based on registration of the heat signal related to freezing and thawing of the water held in the hardened cement paste (Bager and Sellevold 1986a, 1986b; Snyder and Bentz 2004; Sun and Scherer 2010; Wu and Johannesson 2014; Wu *et al.* 2014; Kurumisawa 2015). This method is also used to evaluate the continuity of pores in cement-based materials (Snyder and Bentz 2004). Only few studies include both these two methods (Yonemura *et al.* 2015), and no studies have investigated the difference in measurement results of hardened cement paste equilibrated at different relative humidity conditions. Therefore, the present study aims at clarifying the application limits of low-temperature DSC and proton NMR as regards detecting water held in hardened cement paste at different relative humidities.

Table 1 Composition of white Portland cement (wt%).

	SiO_2	Al_2O_3	Fe_2O_3	CaO	MgO	SO_3	Na_2O	K_2O
WPC	22.9	4.47	0.20	67.96	1.13	2.87	0.23	0.06

2. Experimental details

2.1 Materials used and sample preparation

The cement used in this study was white Portland cement (WPC). It has a low iron content and was chosen for the sake of proton NMR measurement. Pure water conforming to the Japanese Industrial Standard JIS K0557 (JSA 1998) was used as mixing water. The WPC has a solid density of 3.05 g/cm^3, a Blaine specific surface area of 3510 cm^2/g, and the chemical composition shown in **Table 1**. The water cement ratio (W/C) was 0.5. Mixing was done in a standard epicyclical 5-liter Hobart mixer. Specimens for low-temperature DSC measurement were cast in Teflon tubes with an inner diameter of 14 mm and a height of 50 mm, whereas tubes for proton NMR measurement had a diameter of 8 mm and a height of 40 mm. After 1 day of hardening the specimens were de-

[1]Associate Professor, Faculty of Engineering, Hokkaido University, Kita 13, Nishi 8, Kita-ku, Sapporo, Hokkaido 060-8628, Japan. *Corresponding author,
E-mail: kurumi@eng.hokudai.ac.jp
[2] Professor, Department of Civil Engineering, Technical University of Denmark, DK-2800 Kgs. Lyngby, Denmark.

moulded and subsequently cured in water at 20°C for 3 months. Finally, the samples were allowed to equilibrate for at least 3 months at different relative humidities by the saturated salt solution method. At this time, the mass change of each sample at any relative humidity environment was less than 0.02% per day. The sample referred to as equilibrated at 100% relative humidity (RH) was not exposed to drying after water curing.

2.2 Measurements

2.2.1 Thermoporometry by low temperature DSC measurement

After curing 100% RH samples had excess surface water wiped off with absorbent paper, whereas other samples were used with no further treatment. To carry out a measurement a sample was inserted into a cylindrical metal container ("sample holder") just large enough to accommodate the sample. About 10 mg AgI was added as a nucleating agent to the surface of the cement paste to minimize supercooling of water during temperature lowering. A lid was put on the metal container, which was finally inserted into the low temperature differential scanning calorimeter (Calvet Micro Calorimeter, SETARAM BT 2.15). Measurements were done relative to an identical, empty metal container (Bager and Sellevold 1986a). Each sample was exposed to a single measurement cycle where temperature at a rate of 3.3°C/h was changed from 10°C to -55°C, and back again to 10°C. This minimum temperature of -55°C was used as no heat exchange due to water/ice phase change has been observed at lower temperatures (Bager and Sellevold 1986a, 1986b). The pore size distribution was calculated based on the amount of frozen water during temperature lowering and the amount of melted ice during temperature increase. Assumptions and procedures for this calculation are described in previous research (Sun and Scherer 2010). In the present study, pores are assumed cylindrical, and the thickness of the non-freezable water layer is assumed to be 0.8 nm. The formulas used are those shown in Eqs. (1) to (5),

$$r_{freeze} = \frac{64.67}{\Delta T} + 0.57 \quad (1)$$

$$r_{melt} = \frac{32.33}{\Delta T} + 0.69 \quad (2)$$

$$\Delta H_{freeze} = 332.4 \quad (3)$$

$$\Delta H_{melt} = 333.8 + 1.797\Delta T \quad (4)$$

$$v_{pore} = v_{ice}\left(\frac{r}{r-0.8}\right)^2 \quad (5)$$

where r_{freeze} and r_{melt} are pore radii (nm) during freezing and thawing respectively, ΔT is the temperature difference (K) from 273.15 K, ΔH_{freeze} and ΔH_{melt} are the heat exchange during freezing of water and thawing of ice (J/g) respectively, v_{pore} is the pore volume (ml), v_{ice} is the ice volume (ml), and r is the pore radius (nm).

2.2.2 Proton NMR measurement

In ^{1}H NMR measurement, first, excess water above the test tube of 100% RH sample was discarded. Other samples were used with no further treatment. Two measurements, CPMG method and solid echo method, were applied and the relaxation time T_2 was observed (Muller *et al.* 2013a). The CPMG method can mainly measure protons in a liquid state, and the solid echo method can separate protons in a solid component and a liquid component. In this measurement, a 0.47 Tesla main field NMR apparatus was used. It is known that the paramagnetic elements in cement causes line broadening and reduces resolution particularly of high-field NMR, so a low-field NMR device was used (Scrivener *et al.* 2016; McDonald *et al.* 2017). In the solid echo method, the 90° pulse was 2.92 μs, the pulse interval (90° - τ - 90°) is 8.64, 15, 20, 30, 40 μs, the number of data observation points is 1024 times or more, the number of scans is 64, and the waiting time for repetition is 0.5 s. With the solid echo method, it is possible to separate chemically bound water and free water. This was done according to previous research (Scrivener *et al.* 2016). Solid echo data are fitted as the sum of a Gaussian part and an exponential decay by the following equation,

$$M(t,\tau) = A_{solid} \cdot \exp\left[-\left(\frac{t-\tau}{\sigma}\right)^2\right] + A_{liquid} \cdot \exp\left(\frac{-t}{T_2}\right) \quad (6)$$

where $M(t,\tau)$ is the NMR signal at the observation time t, A_{solid} is the signal intensity of solid water, τ is the time of the center of the Gaussian part and σ is its width, A_{liquid} is the signal intensity of liquid water, and T_2 is the relaxation time. For the separation of liquid and solid-like water at $\tau = 0$, an exponential function was used for the back extrapolation, and the ratio of chemically bound water was calculated by approximation using all measured τ values (Scrivener *et al.* 2016).

In the CPMG method, the 90° pulse was 2.5 μs and the 180° pulse was 5.0 μs, the pulse interval (90° - τ - 180°) is 40 μs, the number of recorded echoes in the CPMG echo train is 256, the time between observation points is 85 μs, the number of scans is 32 times, and the waiting time of repetition was set at 5 s. In addition, it was confirmed in a preliminary study that the number of integrations gave a sufficient S/N ratio for analysis. In some of the previous studies, measurements were performed by changing τ, but preliminary to the present study, tests were conducted which confirmed that there is no difference between the results obtained based on a single τ (Scrivener *et al.* 2016). For this reason, the analysis in this study is based on measurements with a single τ. The Contin method (Provencher 1982) and the discrete method (Provencher 1976) have been proposed for the analysis (Scrivener *et al.* 2016). In the present study, the discrete method is used, in which the curve obtained by NMR measurement is represented by the sum of several

components *i* as shown in the following formula,

$$M_{y'}(t) = \sum_{i=1}^{N} M_0^i \cdot \exp\left(\frac{-t}{T_2^i}\right) \quad (7)$$

where, $M_{y'}(t)$ is the NMR signal at the observation time *t*, M_0^i is the NMR signal of the i^{th} component at the observation time of 0 seconds, and T_2^i is the relaxation time of the i^{th} component. In the present study, the number of components was not fixed and the best approximation result was used for the analysis.

2.2.3 Evaporable water and chemically bound water

The moisture content, i.e. "evaporable water" was calculated from the mass loss of crushed sample on heating up to 105°C, and the chemically bound water was calculated from heating in the range 105°C to 950°C. Regarding the degree of saturation, its value at each relative humidity was calculated as the evaporable water relative to the moisture content at saturated surface-dry state. In addition, the crushed sample was ball-milled into powder and used for XRD measurement. The phase composition of the results obtained by XRD measurement was quantified by Rietveld analysis (Doebelin and Kleeberg 2015), and the amount of chemically bound water was corrected by the amounts of water in ettringite and CO_2 in calcite quantified by the method.

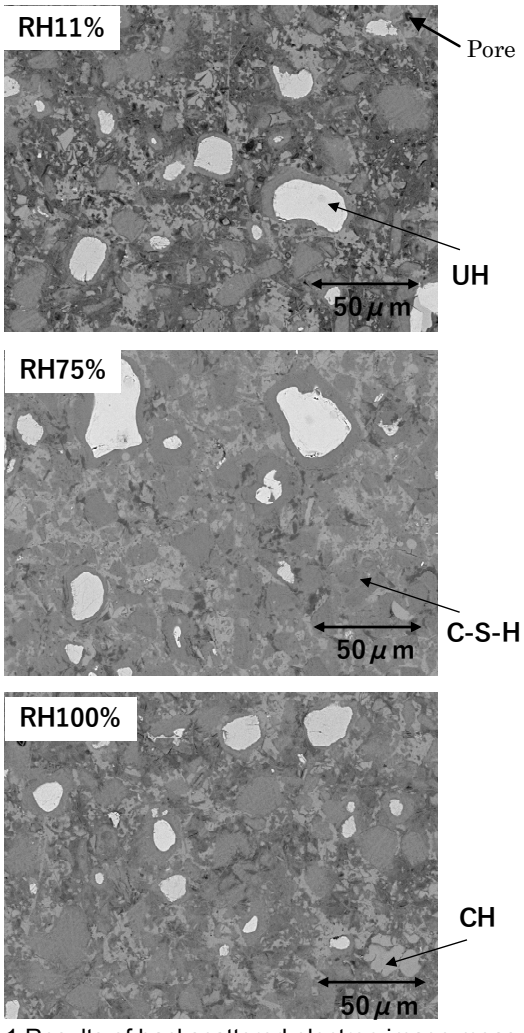

Fig. 1 Results of backscattered electron image measurement at different relative humidities.

2.2.4 Backscattered electron image measurement

A sample was cut into $(5\ mm)^3$ cubes from a specimen that had reached the prescribed age, embedded in epoxy resin and its surface was polished. By observing the surface after polishing with backscattered electron imaging, due to the difference in brightness of each phase, unreacted cement (UH), calcium hydroxide (CH), a hydrate phase (C-S-H) and a coarse pores (Pore) were quantified. However, due to the resolution of the electron microscope, the size of one pixel, 0.32 μm, limits identification of phases with smaller geometry. In addition, the fraction of each phase was obtained by taking 16 or more images with a size of 200 × 150 μm and using the average value. The degree of hydration was determined by including measurements of unreacted cement.

3. Results and discussion

3.1 Backscattered electron imaging, evaporable water and degree of saturation

Figure 1 shows an example of measurement results of backscattered electron imaging of hardened cement paste equilibrated at different relative humidity conditions. The white part is unreacted cement, light gray is calcium hydroxide, and dark gray is hydrate phase containing C-S-H. The residual amount of unreacted cement observed in the backscattered electron image was 2% to 5%, and unreacted cement remained in the low relative humidity samples. The degree of hydration varied from 85% (RH 11%) to 93% (water cured), as a consequence of the different relative humidity conditions during equilibration affecting cement hydration subsequent to the initial 3 months of water curing.

Figure 2 shows the measurement results of evaporable water and degree of saturation of hardened cement paste equilibrated at different relative humidities. For the hardened cement paste used in this study, the evaporable water decreased with decreasing relative humidity, and the degree of saturation also decreased, to the same extent as in previous studies (Maruyama 2010).

3.2 Low temperature DSC

3.2.1 Freezing process

Figure 3 shows the low-temperature DSC measurement results on hardened cement paste during temperature lowering. For larger pore sizes its contained water freezes at higher temperatures, and similarly heat exchange is observed at lower temperatures for smaller pores. An exothermic peak is observed near -5°C in the saturated sample, and further exothermic peaks are also seen around -15°C, -25°C, and -42°C. The freezing

temperature of the water defines the pore type (Snyder and Bentz 2004). Capillary pore water freezes in the range 0 to -20°C, gel pore water between low density (LD) to high density (HD) C-S-H freezes in the range -20 to -30°C, gel pore water in LD C-S-H freezes in the range -30 to -45°C. As seen capillary pore water is observed for the sample equilibrated at 98% RH. Gel pore water frozen in the range of -20 to -30°C is found at RH levels above approximately 80%, whereas below this level only gel pore water in LD C-S-H is present. Furthermore, no clear peak was detected at 33% RH and below.

The temperature at which the first peak occurs is independent of pore size, because pore water freezing occurs due to heterogeneous nucleation during initial cooling (Ishikiriyama *et al*. 1995). Therefore, the pore size distribution cannot be calculated from the freezing process. In order to solve this problem, a measurement method using an auxiliary cycle has been proposed (Ishikiriyama *et al*. 1995; Koniorczyk *et al*. 2018; Bednarska and Koniorczyk 2020), but it was not adopted in this study because of its detrimental effect on the specimen.

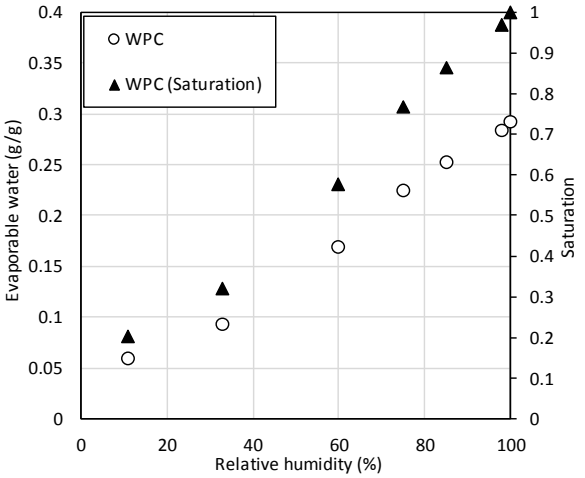

Fig. 2 Relationship between relative humidity of hardened cement paste, evaporable water and degree of saturation.

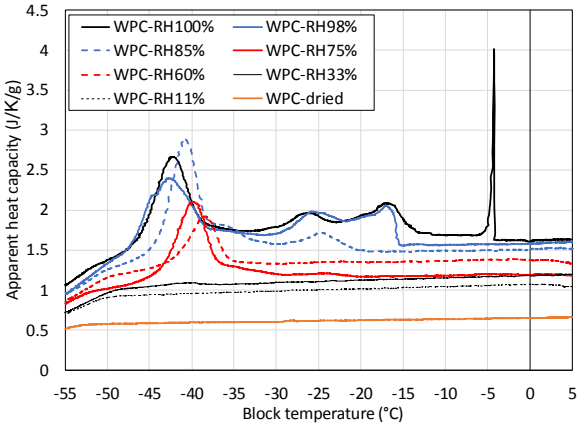

Fig. 3 Low-temperature DSC measurements during temperature lowering of hardened cement paste samples equilibrated at different relative humidities.

3.2.2 Melting process

Figure 4 shows the low-temperature DSC measurement results during temperature increase. Water (in the form of ice) present in the fine pores melts at low temperatures, whereas the large peak near 0°C represents water in relatively large pores. As seen the amount of water-filled coarse pores are reduced as the equilibration RH is lowered. In accordance with the freezing process, no clear peak is detected in samples with an equilibration RH of 33% or less. Comparing the freezing and thawing processes, the peaks detected at -40°C in the freezing process should have been detected at -20°C in the thawing process, but no large peaks were detected. This may be due to the effect of nucleation or the presence of bottle-neck pores.

Figure 5 shows the freezable water content calculated by Eq. (2) applied to the measurement results of the melting process. Note that this is the pore size distribution of the water-filled pores. As seen, when the equilibrium RH is reduced the sample will contain less water-filled porosity. Certainly, thermoporometry based on low-temperature DSC registers only a part of the total

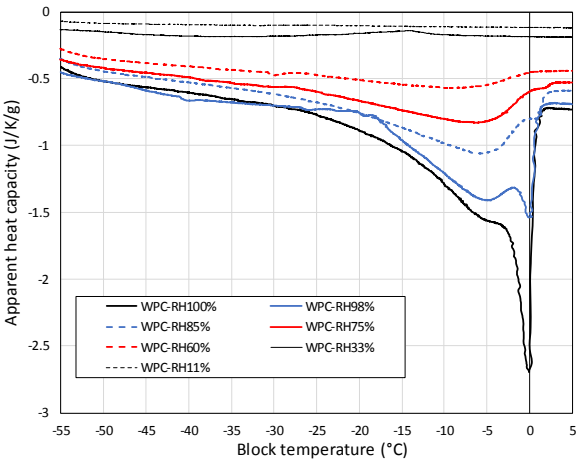

Fig. 4 Low temperature DSC measurement during temperature increase of hardened cement paste samples equilibrated at different relative humidities.

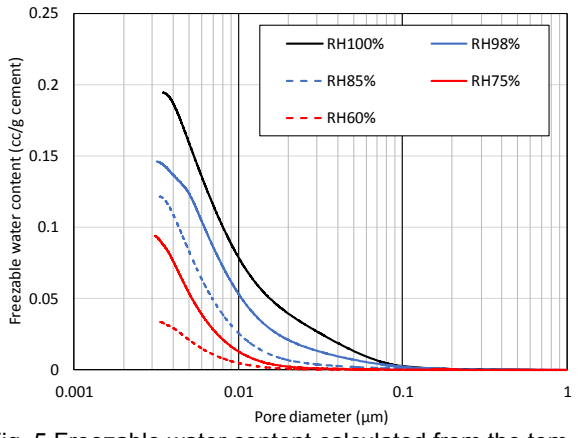

Fig. 5 Freezable water content calculated from the temperature increase process.

pore volume when measurements are done on non-saturated samples. Additionally, as no peaks are detected at equilibration relative humidities of 33% or less, an analysis of the pores related to hardest bound evaporable water is not possible with this measuring technique.

3.3 Proton NMR

3.3.1 Solid echo method

Figure 6 shows the results measured by the solid echo method. Strongly bound and constrained protons have a fast decay, whereas protons that can move more freely have a slower decay. It can be seen that almost the same signal is detected in the test specimens equilibrated at relative humidities of 60% or more. On the other hand, when the equilibrium RH is lowered to 33% or less, the attenuation rapidly decreases, i.e. the protons are less able to move at these low RH levels.

As described previously the registered signal by the solid echo method can be separated as to quantify chemically bound water and free water (i.e. evaporable water). **Figure 7** shows these results. The figure also shows the results of chemically bound water based on 105 to 950°C heating. The two completely different measuring techniques give results that with some uncertainty agree with each other. The amount of chemically bound water is relatively independent of the equilibrium RH, whereas the evaporable water decreased with a lowering in the equilibrium RH. The amount of bound water obtained by proton NMR is slightly lower than the amount of chemically bound water obtained from heating. As pointed out in a previous study (Holthausen and McDonald 2020), the separation of protons in solids and protons in liquid seems to need further improvement. The sample equilibrated at 98% RH showed the highest amount of chemically bound water, because hydration proceeded during the RH equilibration.

3.3.2 CPMG method

Figure 8 shows the results by the CPMG method. The CPMG method can detect the state of evaporable water. For the saturated samples water-filled pores were detected, but unsaturated samples may also have pores detected that were not water-filled. In other words, water that is strongly constrained on the pore surface is detected at all humidity conditions. The fast decay component is linked to protons in water within the range of a solid surface, and the slow decay component is linked to relatively free-moving protons as in water, which is not significantly affected by a solid surface. The maximum value of the detected signal decreases as the equilibration RH decreases, and only the components with faster decay are detected in the low RH equilibrated samples.

Figure 9 shows the result of separating the compo-

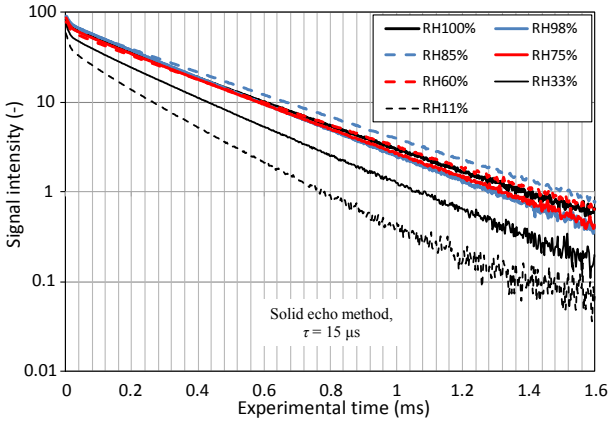

Fig. 6 Proton NMR measurement results of hardened cement paste (solid echo method).

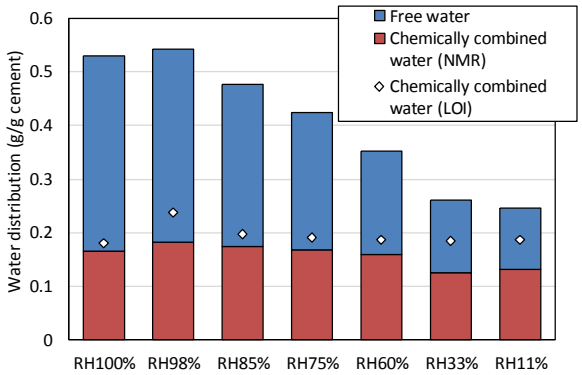

Fig. 7 Proton distribution in hardened cement paste (solid echo method).

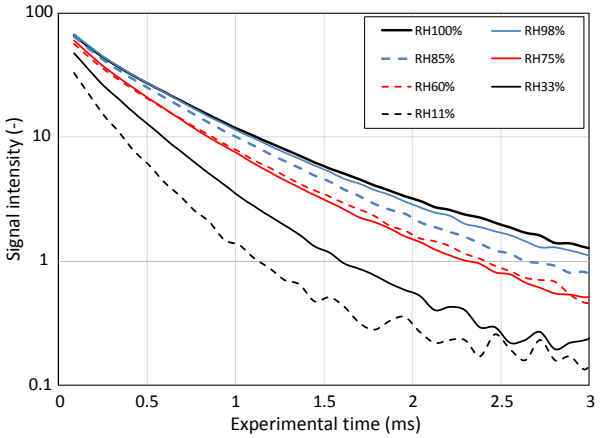

Fig. 8 Proton NMR measurement results of hardened cement paste (CPMG method).

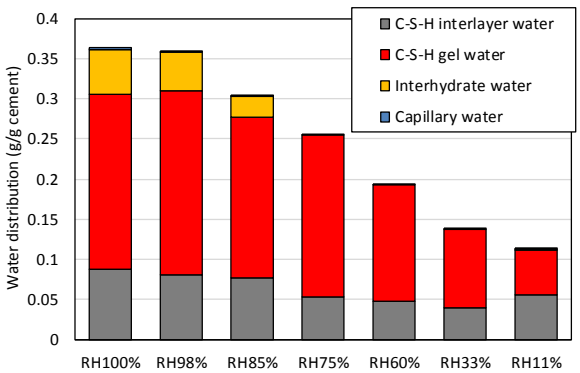

Fig. 9 Proton distribution in hardened cement paste (CPMG method).

nents in free water according to the classification of Muller (Muller *et al*. 2013b; Scrivener *et al*. 2016). The amount of capillary pore water is small in all samples, and water existing between hydrates (inter-hydrate water) is present in samples equilibrated at a RH of 85% or more, and gel pore water and C-S-H interlayer water are present at all equilibration relative humidities. It can be seen that the amount of gel pore water decreases markedly as the equilibrium RH decreases.

3.4 Comparison of low temperature DSC and proton NMR

Comparing **Fig. 2** with **Fig. 5**, the water registered by low temperature DSC, is clearly seen to be only a part of the evaporable water since non-freezable water cannot be detected by this technique. Water held at RH levels of 33% and below seems to be of this type due to its proximity to the solid surfaces. It will be the harder bound gel water and interlayer water. For samples equilibrated at a low RH of 11% and 33%, a proton NMR signal is detected. The amount of water obtained by low-temperature DSC measurement is comparable to the values obtained by NMR (**Fig. 7**) if the amount of water at an equilibration RH of 33% is subtracted. On the other hand, since the absolute amount of water cannot be measured by proton NMR, it is necessary to establish such a relation through a supplementary measurement as for example mass loss in the range from 105 to 950°C.

Gel water was detected by low-temperature DSC measurement in the high RH range of 85% and above, which corresponds to inter-hydrate water detected by proton NMR. However, when the equilibrium RH was 98% or more, the capillary pore water frozen at a temperature higher than -20°C was clearly differentiated by the low temperature DSC, whereas proton NMR is hardly able to detect capillary water as a separate category. It might be that water detected as inter-hydrate water with proton NMR also includes water corresponding to the capillary pore water by low temperature DSC.

From the presented measurements, it is seen that proton NMR is a very useful technique with a broad ability to measure water binding and thus also pore structure in cementitious systems. However, it has to be pointed out that the relaxation time will change significantly if the specimen to be measured contains a large amount of iron or aluminum (McDonald *et al.* 2017; Kurumisawa 2019). In the present study white Portland cement was used, but for many cements, including blended cements, the Proton NMR technique will be less useful or even difficult to apply. In such cases low-temperature DSC may be a more relevant technique.

4. Conclusion

Based on the observations the following main conclusions are suggested:

(1) Low-temperature DSC detects only a part of the evaporable water in hardened cementitious materials, in particular water bound at relative humidities of 33% or less is not detected by this technique. This will include some of the gel pore water and interlayer water in C-S-H.

(2) For the cementitious system examined in the present study proton NMR is able to detect a broad range of water binding, including water held at relative humidities of 33% and below.

(3) Low temperature DSC and proton NMR seem to detect different capillary pore volumes under the high humidity condition of 98% relative humidity.

Acknowledgements

Part of this research was supported by the Research Grant of the Japan Concrete Institute. Part of the NMR measurements was done with equipment at Gunma University Instrument Analysis Center. This is gratefully acknowledged.

References

AIJ, (2018). "*JASS 5: Japanese architectural standard specification for reinforced concrete work*." Tokyo: Architectural Institute of Japan. (in Japanese)

Bager, D. H. and Sellevold, E. J., (1986a). "Ice formation in hardened cement paste, Part I - Room temperature cured pastes with variable moisture contents." *Cement and Concrete Research*, 16(5), 709-720.

Bager, D. H. and Sellevold, E. J., (1986b). "Ice formation in hardened cement paste, Part II - Drying and resaturation on room temperature cured pastes." *Cement and Concrete Research*, 16(6), 835-844.

Bednarska, D. and Koniorczyk, M., (2020). "Freezing of partly saturated cementitious materials - Insight into properties of pore confined solution and microstructure." *Construction and Building Materials*, 251, Article ID 118895.

Brun, M., Lallemand, A., Quinson, J. F. and Eyraud, C., (1977). "A new method for the simultaneous determination of the size and shape of pores: The thermoporometry." *Thermochimica Acta*, 21(1), 59-88.

Doebelin, N. and Kleeberg, R., (2015). "Profex: A graphical user interface for the Rietveld refinement program BGMN." *Journal of Applied Crystallography*, 48, 1573-1580.

Holthausen, R. S. and Mcdonald, P. J., (2020). "On the quantification of solid phases in hydrated cement paste by ^{1}H nuclear magnetic resonance relaxometry." *Cement and Concrete Research,* 135, Article ID 106095.

Ishikiriyama, K., Todoki, M., Kobayashi, T. and Tanzawa, H., (1995). "Pore size distribution measurements of poly (methyl methacrylate) hydrogel membranes for artificial kidneys using differential scanning calorimetry." *Journal of Colloid and Interface Science*, 173(2), 419-428.

JSA, (1998). "*JIS K0557: Water used for industrial water and wastewater analysis*." Tokyo: Japanese Standards

Association.

Kose, Y., Takahashi, T., Tanaka, T. and Ohkubo, T., (2013). "Observation of time-dependent behavior of micro-pore structures in cement paste using ^{1}H NMR." *Concrete Research and Technology*, 24(3), 67-73. (in Japanese)

Koniorczyk, M., Bednarska, D., Nowosielska, M. and Rynkowski, J., (2018). "Nucleation model for mesopore-confined water freezing kinetics." *International Journal of Heat and Mass Transfer*, 120, 575-586.

Kuhn, W., Peterli, E. and Majer, H., (1955). "Freezing point depression of gels produced by high polymer network." *Journal of Polymer Science*, 16(82), 539-548.

Kurumisawa, K., (2015). "Application of thermoporometry for evaluation of properties of hardened cement paste." *Construction and Building Materials*, 101, 926-931.

Kurumisawa, K., (2019). "Relaxation time of hardened cement paste measured by proton NMR and transport properties." In: J. Gemrich, Ed. *Proceedings of the 15th International Congress on the Chemistry of Cement*, Prague, Czech Republic 16-20 September 2019. Prague: Guarant International.

Kurumisawa, K. and Jensen, O. M., (2020). "Measurement of cement paste at different humidities by thermoporometry and proton NMR." *Proceedings of the Japan Concrete Institute*, 42, 347-352. (in Japanese)

Landry, M. R., (2005). "Thermoporometry by differential scanning calorimetry: Experimental considerations and applications." *Thermochimica Acta*, 433(1-2), 27-50.

Maruyama, I., (2010). "Origin of drying shrinkage of hardened cement paste: Hydration pressure." *Journal of Advanced Concrete Technology*, 8(2), 187-200.

Maruyama, I., Ohkubo, T., Haji, T. and Kurihara, R., (2019). "Dynamic microstructural evolution of hardened cement paste during first drying monitored by ^{1}H NMR relaxometry." *Cement and Concrete Research*, 122, 107-117.

McDonald, P. J., Gajewicz, A. M. and Morrell, R., (2017). "Good practice guide 144: The characterisation of cement based materials using T2 ^{1}H nuclear magnetic resonance relaxation analysis." Middlesex, UK: National Physical Laboratory.

Muller, A. C. A., Scrivener, K. L., Gajewicz, A. M. and McDonald, P. J., (2013a). "Densification of C-S-H measured by ^{1}H NMR relaxometry." *Journal of Physical Chemistry C*, 117(1), 403-412.

Muller, A. C. A., Scrivener, K. L., Gajewicz, A. M. and McDonald, P. J., (2013b). "Use of bench-top NMR to measure the density, composition and desorption isotherm of C-S-H in cement paste." *Microporous and Mesoporous Materials*, 178, 99-103.

Muller, A. C. A., Scrivener, K. L., Skibsted, J., Gajewicz, A. M. and McDonald, P. J., (2015). "Influence of silica fume on the microstructure of cement pastes: New insights from 1H NMR relaxometry." *Cement and Concrete Research*, 74, 116-125.

Provencher, S. W., (1976). "An eigenfunction expansion method for the analysis of exponential decay curves." *The Journal of Chemical Physics*, 64(7), 2772-2777.

Provencher, S. W., (1982). "Contin: A general purpose constrainded regularization program for inverting noisy linear algebraic and integral equations." *Computer Physics Communications*, 27(3), 229-242.

Scrivener, K., Snellings, R. and Lothenbach, B., (2016). "*A practical guide to microstructural analysis of cementitious materials*." London and New York: CRC Press.

Snyder, K. A. and Bentz, D. P., (2004). "Suspended hydration and loss of freezable water in cement pastes exposed to 90% relative humidity." *Cement and Concrete Research*, 34(11), 2045-2056.

Sun, Z. and Scherer, G. W., (2010). "Pore size and shape in mortar by thermoporometry." *Cement and Concrete Research*, 40(5), 740-751.

Yonemura, M., Kitagaki, R., Ohkubo, T. and Kim, J., (2015). "Pore structure analysis of hardened cement using ^{1}H NMR." *Proceedings of the Japan Concrete Institute*, 37(1), 511-516. (in Japanese)

Wu, M. and Johannesson, B., (2014). "Impact of sample saturation on the detected porosity of hardened concrete using low temperature calorimetry." *Thermochimica Acta*, 580, 66-78.

Wu, M., Johannesson, B. and Geiker, M., (2014). "A preliminary study of the influence of ions in the pore solution of hardened cement pastes on the porosity determination by low temperature calorimetry." *Thermochimica Acta*, 589, 215-225.